Design of a Doubly-Fed Reluctance Motor for Adjustable Speed Drives

Yuefeng LIAO

Advanced Motor Development Center
Emerson Motor Co.
8100 W. Florissant Ave.
St. Louis, MO 63136

Li ZHEN and Longya XU

Department of Electrical Engineering
The Ohio State University
2015 Neil Avenue
Columbus, Ohio 43210

Abstract - **A methodology for steady-state performance analysis and design of the doubly-fed reluctance motor (DFRM) is presented in this paper. Emphasis is placed on the linear model of the DFRM, but magnetic nonlinearities are also characterized. A prototype 2 hp DFRM is designed and built in comparison with an induction motor. Performance of the prototype 2 horsepower DFRM motor is analyzed thoroughly and is supported by actual measurements, wherever available.**

I. INTRODUCTION

Recently, interest in the brushless doubly-fed motors to be used in adjustable speed drives (ASD's) has been revived [1-13]. Although these motor concepts, which evolved from the well-known technique of cascaded connection of induction motors, had been extensively investigated two decades ago by Broadway and his associates [14-15], the technical and economical context has since then changed so much with the fusion of Electromechanics, Power Electronics and Motion Controls that the potential of these brushless doubly-fed machines warrant re-examination in the new framework of perspective. The motivation behind these efforts is to drive to minimum the cost of the power converters, which remains the major contributor of a ASD system, while retaining the desirable feature of brushless operation. The brushless doubly-fed motors/drives embody such a unique combination. From the perspective of a motor design specialist, since each of these doubly-fed motors is a compromise of two motors of different pole-number sharing the same magnetic path and slot space, its performance has to suffer despite of the designer's ingenuity. As a result, a cost penalty may have to be paid on the motor side. However, this cost differential on the motor side usually can well be justified in the cost equation of the whole system, resulting in an economically more favorable combination over the well-known solution of induction motor drives [16]. This constitutes an economically attractive approach for the vast market of pump-type applications with which the required speed variation is limited

Thus far, attention has mainly been focused on the development of the brushless doubly-fed (induction) machine (BDRM) with a specially designed cage on the rotor [1-2, 8-11], and the doubly-excited brushless reluctance machine (DEBRM) with an axially-laminated rotor [3,5-7]. The Doubly-Fed Reluctance Machine (DFRM) with simple saliency on the rotor has been relatively overlooked despite its structural simplicity, lower manufacturing cost and compatibility with existing production lines. This has resulted from both theoretical and technical difficulties. Theoretically, the DFRM differs substantially from the brushless doubly-fed induction machine and defies the semi-intuitive approach which had long been used for analysis of the BDRM. It is until recently that an attempt was made to give a rigorous and complete analysis of such machines based on winding function theory [4-5]. Unfortunately, the effect of the weak coupling between the two sets of stator windings, which determines the synchronous machine behavior of such doubly-fed reluctance machines, remains obscure in these prior works. Technically, it is well understood that reluctance motors will exhibit very poor performance without proper control of the current. The same is true for the DFRM fed by a simplistic voltage-source converter. These two obstacles had long hindered in-depth exploration of the full potential of such deceptively simple DFRM motors until very recently, a rigorous yet physically insightful approach based on the concept of spatially modulated revolving field was adopted and a sensorless control was devised by one of the authors [12-13]. It has been demonstrated that with proper control of the winding currents, the DFRM behaves in a similar way as a non-salient synchronous machine and closed-looped control can be achieved with a greatly reduced sized power converter. Moreover, equipped with the sensorless control, the DFRM drive can be applied to restricted applications where accessibility to the rotor shaft is prohibited.

This paper is intended to address the design issues in the development of the DFRM. To provide a sound basis for design of such DFRM machines, the basic electromagnetic relationships of the DFRM are first derived with the aid of the concept of spatially modulated revolving field, which has long been used for the analysis of harmonic fields of induction machines [17]. The peculiarities of the machine are characterized and visualized to provide insights into the operating principles of the machine. The equivalent circuit of the machine is developed which serves as a basis for design and controls development of the DFRM. The nonlinear behavior of the DFRM is also characterized. A prototype 2 hp DFRM is designed and built and comparison is made between the DFRM and the induction machine housed in the same frame. Performance of a prototype 2 horsepower DFRM motor is analyzed thoroughly and is supported by actual measurements, wherever available.

II LINEAR MODEL OF THE DFRM

A schematic of the DFRM drive is shown in Fig. 1. The DFRM motor has two sets of windings of 2p-pole and 2q-pole, respectively, laid in the stator slots. The 2p-pole windings, named the primary windings, are connected directly to the AC power supply while the 2q-pole windings, or the secondary windings, are fed from a variable frequency power converter, as shown in Fig. 1. The rotor is made of laminated steel having p_r salient poles, without any winding or cage on it.

0-7803-1993-1/94 $4.00 © 1994 IEEE

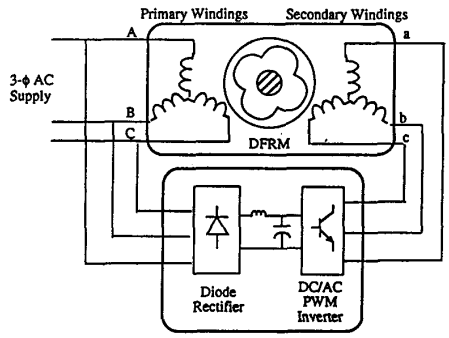

Fig. 1 Schematic of the Doubly-Fed Reluctance Motor Drive

A cross-section view of a typical DFRM is shown in Fig. 2. As a simplification, each of the phase windings in each winding sets can be approximated by a sinusoidally distributed winding function. As shown in Fig. 3, $n_A(\phi)$ represents the A-phase winding of the primary windings and $n_a(\phi)$ represents the a-phase winding of the secondary windings, with N_A and N_a being the

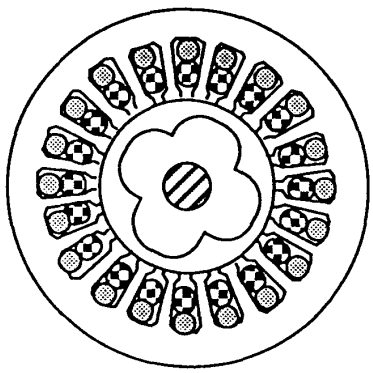

Fig. 2 Cross-Section View of the DFRM

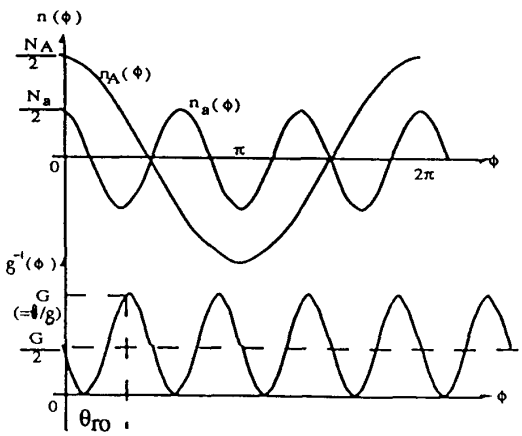

Fig. 3 Variations of Winding Functions and the Inverse Airgap Function

effective series turns per phase per pole pair, respectively. The variation of the airgap length, thus the inverse airgap length g^{-1} as a function of the mechanical angle ϕ, can be approximated as a sine wave biased by the average of the maximum and minimum values of $g^{-1}(\phi)$, as shown in Fig. 3.

$$g^{-1}(\phi) = \frac{G}{2}\,(1+\cos p_r\,(\phi - \theta_r)) \qquad (1)$$

where $G = \frac{1}{g}$, $p_r = 4$ for the case shown.

If a set of symmetrical sine-wave currents of frequency ω_1 and peak value I_M are flowing in the primary windings, and another set of currents of frequency ω_2 and peak value I_m are flowing in the secondary windings, two MMF waves will be set up in the airgap:

$$F_p(\phi) = F_{pm}\cos(\omega_1 t - p\phi) \qquad (2)$$

$$F_s(\phi) = F_{sm}\cos(\omega_2 t - \alpha - q\phi) \qquad (3)$$

with

$$F_{sm} = \frac{3}{2} N_a I_m \quad \text{and} \quad F_{pm} = \frac{3}{2} N_A I_M$$

Neglecting magnetic saturation for the time being, we can find the airgap flux density waves corresponding to the above two MMF waves:

$$B_p(\phi) = B_{pm}\cos(\omega_1 t - p\phi) + B_{pm}\cos(\omega_1 t - p\phi)\cos p_r\,(\phi - \theta_r) \qquad (4)$$

$$B_s(\phi) = B_{sm}\cos(\omega_2 t - \alpha - q\phi) + B_{sm}\cos(\omega_2 t - \alpha - q\phi)\cos p_r\,(\phi - \theta_r) \qquad (5)$$

with

$$B_{pm} = \frac{3}{4}\mu_0 G\,(N_A I_M)$$

$$B_{sm} = \frac{3}{4}\mu_0 G\,(N_a I_m)$$

The second term in each of the airgap flux density waves, $B_p(\phi)$ or $B_s(\phi)$, represents a spatially-modulated sine wave and can be decomposed into two sine waves traveling in opposite directions. Under certain conditions of current frequency, rotor speed and pole number combination, one of these two sine waves will be in synchronism with the first term sine wave generated by the other windings. As a result, energy conversion takes place. This condition can be determined by examining the flux linkage expressions for both stator windings.

The flux linkages of A-phase and a-phase are [18]

$$\lambda_A = \lambda_{Ap} + \lambda_{As} = r l \int_0^{2\pi} B_p(\phi) n_A(\phi) d\phi + r l \int_0^{2\pi} B_s(\phi) n_A(\phi) d\phi \qquad (6)$$

$$\lambda_a = \lambda_{ap} + \lambda_{as} = r l \int_0^{2\pi} B_p(\phi) n_a(\phi) d\phi + r l \int_0^{2\pi} B_s(\phi) n_a(\phi) d\phi \qquad (7)$$

with r and l denoting the radius and the stack length of the rotor.

It can be found that if $p_r = p+q$ and $\omega_r = (\omega_1 + \omega_2)/p_r$, we will have

$$\lambda_A = \lambda_{Ap} + \lambda_{As} = L_p I_M \cos(\omega_1 t) + L_{ps} I_m \cos(\omega_1 t - \alpha + \gamma) \qquad (8)$$

$$\lambda_a = \lambda_{as} + \lambda_{ap}$$
$$= L_s I_m \cos(\omega_2 t - \alpha) + L_{ps} I_M \cos(\omega_2 t + \gamma) \quad (9)$$

with

$$L_p = (\frac{\pi}{2})\frac{3}{4}\mu_0 r l\, G (N_A)^2$$

$$\frac{L_p}{L_{ps}} = 2(\frac{N_A}{N_a})^2, \quad \frac{L_p}{L_s} = (\frac{N_A}{N_a})^2$$

and

$$\gamma = p_r \theta_{ro}$$

If, by proper control, α is kept 180 degree, we will have the following expressions in phasor forms for the back EMF's:

$$\dot{E}_A = \dot{E}_{Ap} + \dot{E}_{As} = -j\omega_1 L_p \dot{I}_A - j\omega_1 L_{ps} \dot{I}_a \angle\gamma \quad (10)$$

$$\dot{E}_a = \dot{E}_{as} + \dot{E}_{ap} = -j\omega_2 L_s \dot{I}_a - j\omega_2 L_{ps} \dot{I}_A \angle\gamma \quad (11)$$

Plus the voltage equations for the primary and secondary windings, we can construct the equivalent circuit of the DFRM as shown in Fig. 4, which bears resembrance to that of the non-salient synchronous machine, especially when the secondary current frequency is zero (i.e. DC excitation).

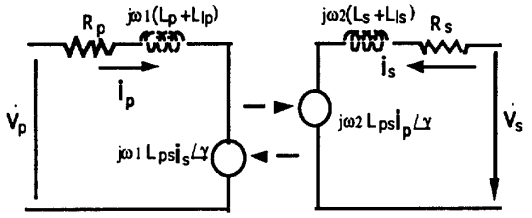

Fig. 4 Equivalent Circuit of the DFRM Motor

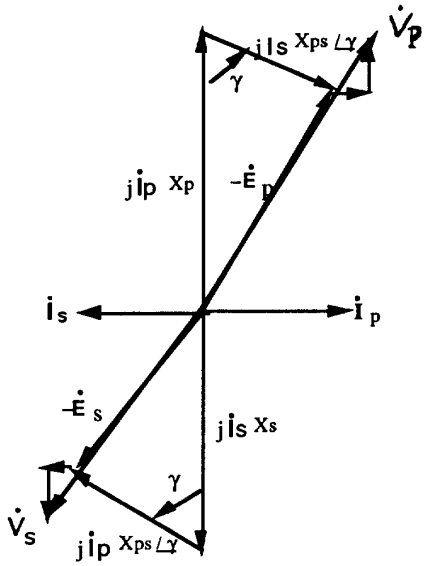

Fig. 5. Phasor Diagram of the DFRM Motor at Rated Load

The torque expression can then be found from the equivalent circuit, by power balance

$$T = \frac{3}{\omega_r}(\dot{E}_{As}\dot{I}_A + \dot{E}_{ap}\dot{I}_a)$$
$$= \frac{3}{2}(p+q)L_{ps}I_m I_M \sin\gamma \quad (12)$$

Eqn (12) clearly shows the synchronous machine torque production mechanism. It is obvious that the DFRM behaves like a non-salient synchronous machine with 2(p+q) poles and the synchronous speed of $\omega 1/(p+q)$. The saliency on the rotor serves only to provide magnetic couplings between the two stator windings. The rotor speed is a function of the frequency of the secondary winding currents and variable speed operation can be realized by controlling the frequency of the secondary winding currents in either open loop or closed loop fashions. Generally, one can identify three modes of operation in the DFRM drive system:

- Sub-synchronous operation where $\omega_2 < 0$;
- Synchronous operation with DC excitation ; and
- Super-synchronous operation where $\omega_2 > 0$.

For instance, for a 2/6-pole machine, ω_2 needs to be changed from $-\omega_1$ to 0 to ω_1 for the motor to start from standstill to rated speed 1800 rpm. (The minus sign indicates opposite phase sequence.)

When the motor is in the sub-synchronous operation mode, a certain amount of electrical energy is dumped back to the DC bus of the power converter. If the motor is intended to run steadily in this speed range, the converter needs to have regenerative capability. However, for most pump-type applications, the variation of the speed is typically 70%-100% rated speed. In this case, the power converter absorbs energy only during start-up, which requires only slight braking capability which is readily provided for in almost all commercial power converters. Also note that the drawback of the DFRM drive is the lack of field-weakening capability since the primary windings are connected to 3-phase 60Hz AC power supply. Hence, it is most suited for pump-type applications.

The corresponding phasor diagram for the case of $\omega_2 = \omega_1$ (i.e. at maximum speed) is shown in Fig. 5 for the purpose of illustration. Observations are in order. It can be seen that the power factor of the DFRM is relatively poor due to the weak coupling between the two sets of stator windings ($L_{ps} = 0.5\, L_p$). This weak coupling leaves the DFRM with a large leakage inductance, which excludes the possibility of line-starting the motor by short-circuiting the secondary windings. It is also clear that the active power is almost evenly distributed among the two sets of windings, while a larger portion of the reactive power is provided from the utility directly through the primary windings. Therefore, the VA ratings of the power converter feeding the secondary windings will be less than half the motor power rating. With such rating, the converter can soft-start the machine even with rated load torque. Also worth mentioning is the reciprocality nature of the DFRM as revealed in Fig. 4&5. In other word, the primary windings and the secondary windings are interchangable and the torque angle, γ, is the same as seen from both side. This latter observation forms the basis for the development of the sensorless control as described in [15].

It is very interesting to note that, unlike synchronous machines, the two fields set up by the two sets of stator windings are not stationary with respect to each other. Rather, these fields

are "locked" into synchronism in such a way that the peaks of the two MMF waves coincide periodically on a pair of rotor poles. To visualize this peculiarity, let's look at a DFRM with p=1, q=3 and p_r=4. Fig. 6&7 show two consecutive instants when the peaks of the two MMF waves meet, for the cases of $\omega_r = 0$ (standstill) and $\omega_r = 900$ (synchronous speed), respectively. The MMF waves due to the two sets of stator currents are represented as the vectors and the torque angle γ is assumed to be zero. Fig. 6 shows the case of standstill, where both the 2- and 6-pole windings are excited by 60 Hz AC currents, abeit with opposite sequences. Originally, the peaks of the 2-pole MMF wave meet one pair of peaks of the 6-pole MMF wave, with one pair of rotor poles underneath. After 1/4 of the time period of the current, the 2-pole MMF wave moves 90 degrees counter clock-wise and the 6-pole MMF wave moves 30 degrees clock-wise, while the rotor remains still. The same field pattern repeats at this time instant, abeit on another pair of peaks of the 6-pole MMF wave, with the other pair of rotor poles underneath.

In another case as shown in Fig. 7, the 6-pole windings are excited by DC while the 2-pole windings by 60 Hz AC, and the rotor is running at 900 rpm in the counter clock direction. The two consecutive locations of repetition will be 120° apart in space, and the time elapsed is 1/3 of the time period of the 2-pole winding current. The rotor, consequently, has to move 30° counter clock-wise to keep in synchronism.

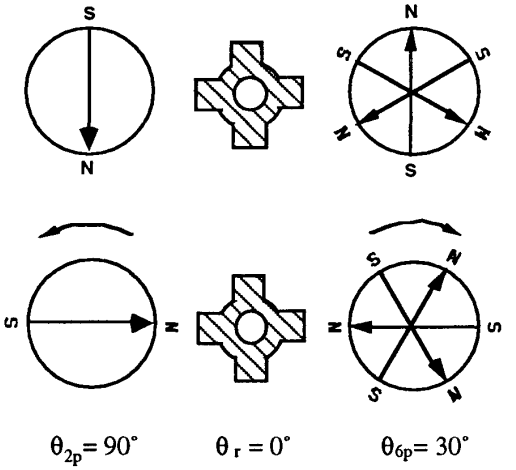

Fig. 6 Movement of Stator MMFs and Rotor Poles at Standstill

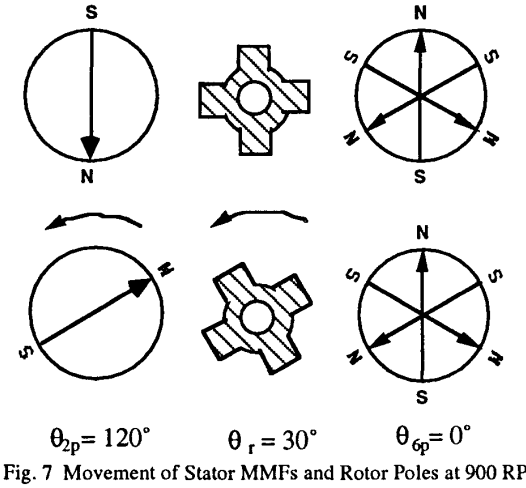

Fig. 7 Movement of Stator MMFs and Rotor Poles at 900 RPM

III. NONLINEAR BEHAVIOR OF THE DFRM

In the foregoing discussion, it is assumed that the DFRM is free of magnetic saturation and the two fields of different pole numbers sharing the same magnetic path are not interfering each other. This is a good approximation of machines with low magnetic loading. In reality, every practical design will place the motor in the modestly saturated regime. Therefore, it is important to characterize the effect of magnetic saturation on the performance of the DFRM to arrive at a good magnetic design.

Compared to the case of brushless doubly-fed induction motors with a uniform airgap, the flux distribution in the DFRM is less regular due to the presence of rotor saliency. It is relatively easier to determine the maximum flux density in the tooth in the worst case, but the flux distributions in the cores depend on the rotor position and the load conditions as well. A conservative approach would be, as in the case of brushless doubly-fed induction motors, to leave sufficient margin to ensure that the teeth and the cores remain unsaturated even in the worst case. This, however, may result in an unnecessarily oversized design. It is interesting to note that with proper control of the secondary currents, the two MMF waves tend to demagnetize against each other. Therefore, magnetic saturation is likely to be much more benign in the DFRM. This suggests that compromise may be made to allow for local saturation to get a more compact design, as long as it will not cause severe degradation of the performance of the motor. To this end, finite element analysis provides a valuable tool.

Finite element analysis was employed to get a good cut in the design of the prototype 2/6-pole DFRM, with its details to be given in the next section. In particular, the primary windings and the secondary windings are designed to have the same ampere-turns per pole with rated currents. Without loss of generality, we need only to look at the synchronous operation. Three load conditions are shown in Table I for the purpose of illustration. Case (I) is the no-load condition where only the primary windings are excited and the secondary windings are left open. The flux contour plot at the starting instant is shown in the figure, with the maximum tooth flux density of 1.80 T and the maximum stator core flux density of 1.60 T. It is clear that the motor is already in modestly saturated without the presence of the secondary currents. Variations of flux linkage for both sets of windings over 90 mechanical degrees of rotor rotation are also shown in the figure. Despite the presence of harmonics, the dominant sinusoidal component in the primary windings and the DC component in the secondary windings are clearly shown, and the magnitude and phase-shift relationships between the primary and secondary winding flux linkages, as dictated by Eqn. (9), are strictly held. Case (II) is a somewhat artificial load condition to show the demagnetizing effect of the secondary current. Full current is applied to the 6-pole secondary windings. Although the local maximum tooth and stator core flux densities reach 1.90 T and 1.70 T respectively, the peak flux linkage in the primary and secondary windings are reduced to around 1/2. The last case shows the full-load condition where the torque angle is 60 degree, with the rotor lagging 15 degrees mechanically. Again the local maximum tooth and stator core flux densities reach 1.85 T and 1.7 T respectively, but the peak flux linkage in the primary and secondary windings all drop by the ratio of $\sqrt{3}/2$, conforming the vectorial relationships as depicted in Fig. 5.

One can conclude that the interaction of the two fields of different pole numbers in a DFRM is of demagnetization nature and will produce mainly local saturation during normal operating conditions. As a result, the assumption of linear magnetics is still valid. However, this local saturation, if aggravated, may result in cross-coupling and other severe secondary effects Detailed analysis of these phenomena is outside the scope of the paper and the reader is refereed to [19] for further discussion.

TABLE I FINITE ELEMENT ANALYSIS OF THE DFRM AT VARIOUS LOAD CONDITIONS

	CASE (I)	CASE (II)	CASE (III)
AIRGAP MMF DISTRIBUTION	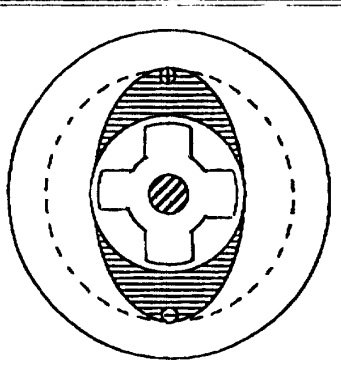	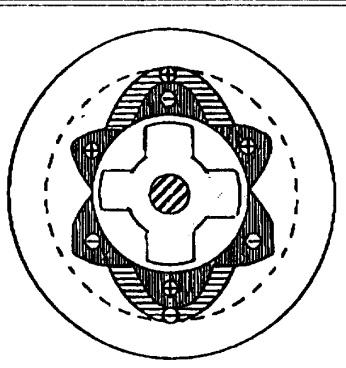	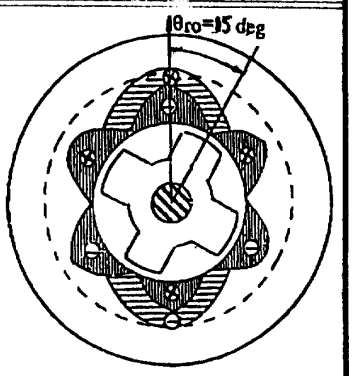
FLUX CONTOUR PLOT	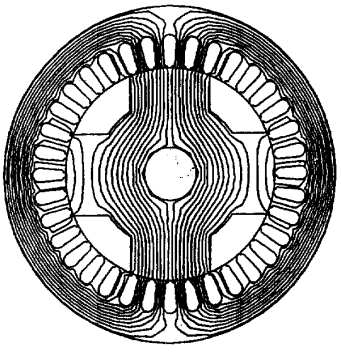	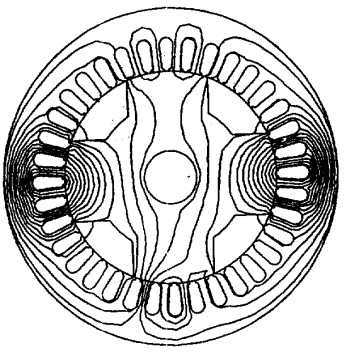	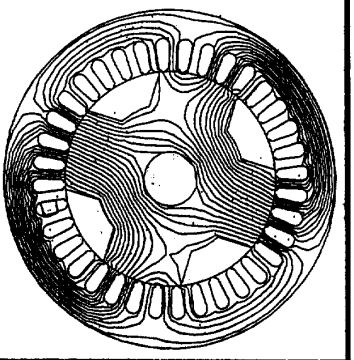
FLUX LINKAGE VARIATIONS (PRIMARY WINDINGS)	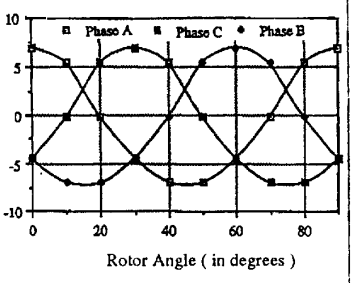	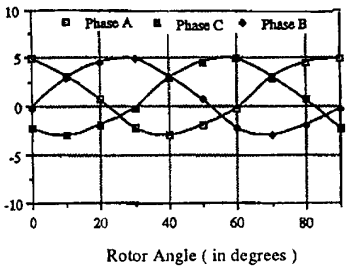	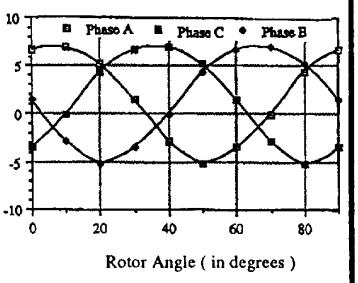
FLUX LINKAGE VARIATIONS (SECONDARY WINDINGS)	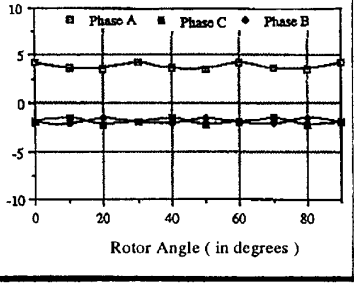	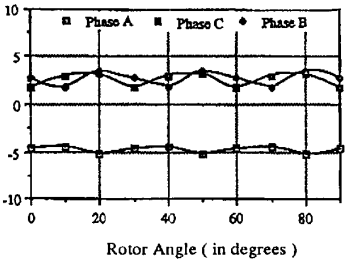	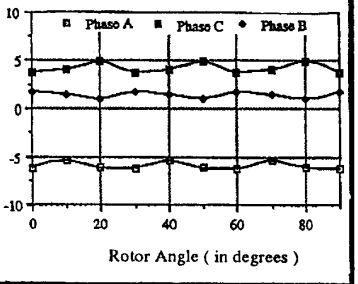

IV DESIGN OF THE PROTOTYPE DFRM

Since the DFRM resembles, in principle, the non-salient synchronous machine, many well-established sizing guidelines and design considerations for the synchronous machine are applicable to the design of the DFRM. Among other factors, the selection of the airgap length is critical to the performance of the DFRM. It can be proved that Xp = 2.0 p. u. is a favorable choice. Due to space limit, the proof is omitted here.

For most ASD systems, a diode bridge rectifying front-end is used and as such, the converter can supply 1/2 (or less) the utility line-to-line voltage. Therefore, it is necessary to select a 2:1 primary/secondary voltage ratio for the DFRM. This selection, however, will not present any difficulty in designing a DFRM with the same ampere-turns per pole for both sets of windings with rated currents. With such design, the active power and the reactive power will be distributed almost evenly between the two sets of windings at maximum speed.

A prototype DFRM of 2/6-pole stator and a 4-pole rotor has been designed to verify the methodology proposed above. With such pole number combination, the DFRM will reach synchronous speed at 900 RPM and will deliver maximum power at 1800 RPM, subject to voltage constraint on the secondary windings. For a meaningful comparison, the prototype DFRM was designed intentionally to have the same outer diameter and stack length as that of a commercial 3 horsepower, 4-pole induction motor housed in a NEMA 180 frame. Decision was made to use the stator lamination of the induction motor for the DFRM, and the airgap length for both motors was kept the same.

As the first iteration, the stator copper losses were maintained the same for both motors. It turned out that the DFRM could only deliver 1/2 the rated torque of the induction motor. Noting that the DFRM is free of rotor copper losses, one can increase the stator currents of the DFRM to keep the total copper losses in both motors the same, as long as the magnetic path remains modestly saturated, which was checked by FEA as described in Section III. This allows the stator currents of the DFRM to be increased by a factor of $\sqrt{2}$ in this case. Unfortunately, the terminal voltage constraints on both stator windings need to be met. Adjustment of the turns were then made and finally, the last iteration of design was arrived. The prototype DFRM built is pictured in Fig. 8, with the rotor laminar also shown in the picture. Main dimensions and performance of final design of the prototype DFRM in comparison with that of the induction motor are summarized in the Table II. It is clear that due to a lower power factor, the DFRM can only deliver 2 horsepower at 1800 RPM.

Table II COMPARISON OF DFRM & IM DESIGNS

	DFRM Design	I M Design
Stator OD (Do)	7.480 inches	(same)
Stator ID (Di)	4.750 inches	(same)
Stack (L_{eff})	3.000 inches	(same)
Airgap (g)	0.013 inches	(same)
Rotor ID (Dri)	1.188 inches	(same)
Voltage	460/230	460
Current	2.01/4.02	3.97
Efficiency(%)	84.0	87.5
Power Factor	0.54	0.80

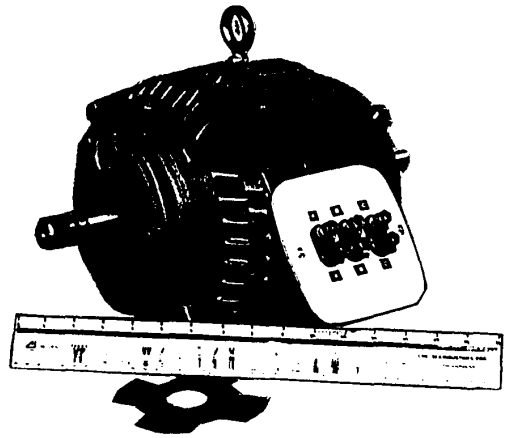

Fig. 6 The Prototype 2 Horsepower DFRM Motor

The part load characteristics of the DFRM are also of interest since the primary windings are now constrained with fixed voltage supply. The variations of the primary and secondary currents as well as the power factor angle on the primary side of the prototype 2 hp DFRM motor under different types of loads are shown in Fig. 7, assuming constant torque angle (60 degrees) control. It can be seen that the primary winding current is almost invariant of load conditions while the secondary current varies in wide range. Also note that the power factor on the primary side drops rapidly with reduced load, similar to that of other types of doubly-fed drive systems [1].

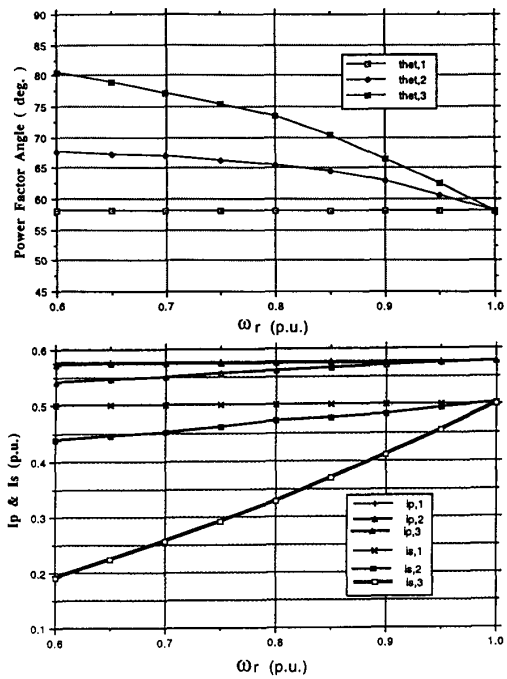

Fig. 7 Steady-State Characteristics of the DERM under Different Load Conditions ($\gamma = 60^{\circ}$)
(1) Constant Torque ($T_l = 1.0$ p.u.);
(2) Fluid Pump-Type Torque ($T_l = 0.8 + 0.2 (\frac{\omega_r}{\omega_B})^2$ p.u.);
(3) Fan-Type Torque ($T_l = (\frac{\omega_r}{\omega_B})^2$ p.u.);

V. EXPERIMENTAL RESULTS

The prototype DFRM has been tested with a proof-of-concept sensorless DFRM drive in the Emerson Advanced Motor Development Center. The control was implemented on a general-purpose digital controller built around a Motorola DSP56000 application development system, as shown in Fig. 8. Seven analog-to-digital channels are used to aquire the primary voltages, primary currents and secondary currents. This system controls a BJT PWM variable speed drive. The sampling rate is around 1.2KHz.

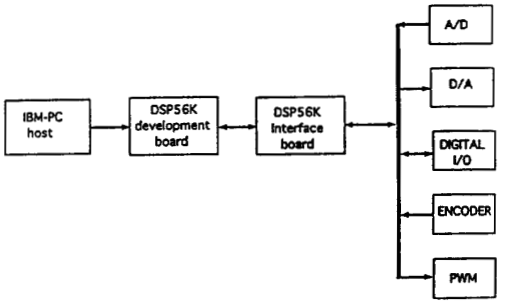

Fig. 8 Motorola DSP56000-Based General Control System

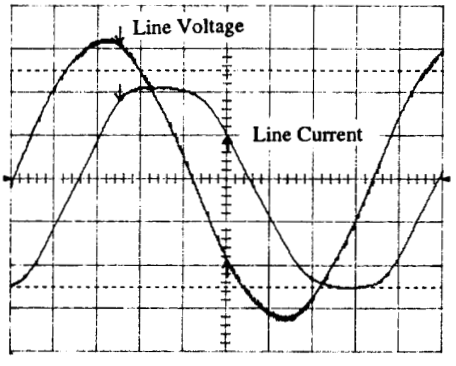

Fig. 9 Line Voltage and Current of the Primary Windings

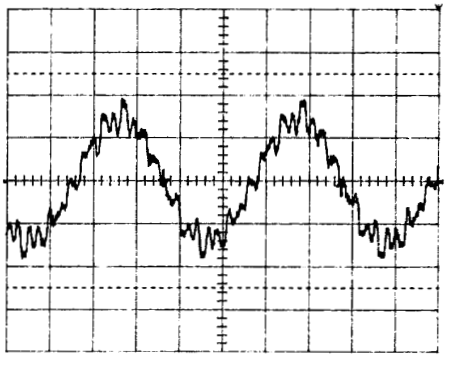

Fig. 10 Back EMF Waveform of the Secondary Windings

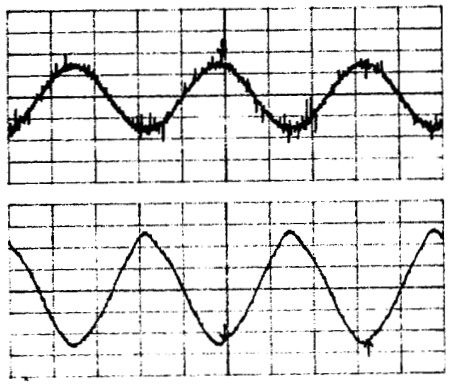

(a) $\omega_r = 0$

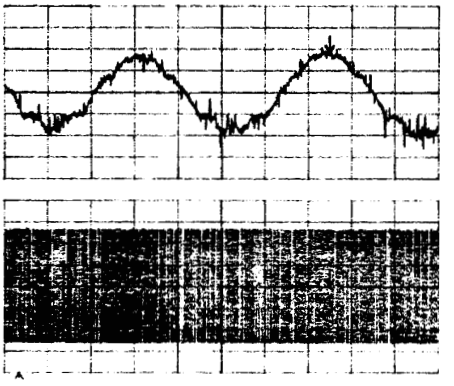

(b) $\omega_r = 910$ rpm

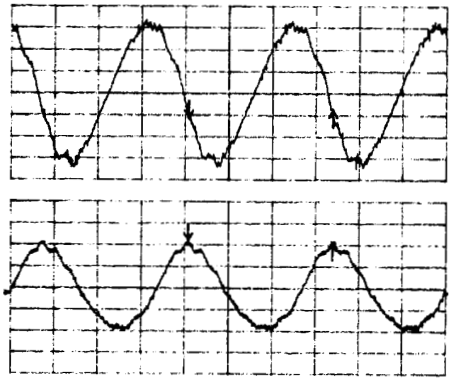

(c) $\omega_r = 1800$ rpm

Fig. 11 Primaryand Secondary Current Waveforms at Different Speeds.
Top trace: Secondary current (2.0 A/div.)
Bottom trace: Primary current (1.0 A/div.)

Figure 9 shows the line voltage and current of the DFRM primary windings at no-load, with the rotor standing still. The distortion of the current waveform is due to the non-sinusoidal

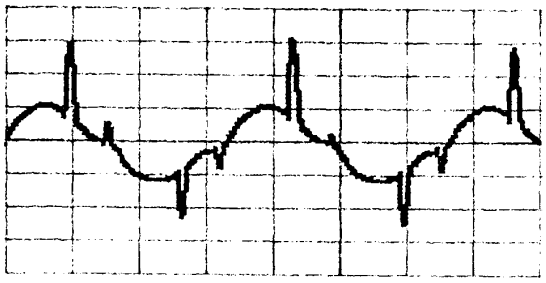

Fig. 12 AC Line Current Waveform of the DFRM Drive

distribution of the airgap. The induced back EMF in the secondary windings is shown in Fig. 10, with the time scale doubled to show the repeatability of the time harmonics due to slotting. Fig. 11 shows the A-phase primary current and a-phase secondary current at zero speed, synchronous speed and maximum speed. It can be observed that the phase-shift between the primary current and the secondary current is well maintained at low speed. However, at maximum speed, due to insufficient DC bus voltage, secondary current control becomes difficult and 180 degree phase-shift can't be strictly held at full current level.

The waveform of the AC line current input to the whole system is shown in Fig. 12. Compared to the typical AC line current waveforms of ASD's with diode rectifier front-ends, it is clear that the line current harmonic distortion of the DFRM drive is much more benign and the effective power factor of the system greatly improved. Performance testing of the DFRM and the drive as a whole is being instrumented and the results will be published in the near future.

VI. CONCLUSION

This paper has presented a methodology for steady-state performance analysis and design of the doubly-fed reluctance motor. It has been demonstrated that with proper control of the winding currents, the DFRM behaves in a similar way as a non-salient synchronous machine. A prototype 2 hp DFRM is designed and built in comparison with an induction motor. It is shown that the power density of the DFRM is 33.3% lower than that of the induction motor due to a lower power factor which is inherent of the operation of the DFRM. However, it should be realized that the prototype DFRM is by no means an optimized design and the comparison tends to be pessimistic. Moreover, the DFRM tends to be of significantly lower cost than that of the induction machine due to simpler rotor assembly and absence of any rotor winding. A thorough evaluation of the performance potential of the DFRM can only come following a detailed sizing analysis and exhausted experimental studies. Work is under way in this direction.

While the DFRM drive still stands out as a promising alternative despite its low power factor, the search for ways to overcome this disadvantage will be the focus on which future research and development will be directed. Among other things, the axially-laminated rotor structure does represent an opportunity for further exploration. Although the scope of the paper is limited to the doubly-fed reluctance motor, the approach presented in this paper also holds promise for the design and controls development of other types of doubly-fed motors/drives, particularly the doubly-excited brushless reluctance motor with axially-laminated rotor structure, in light of the vital role of the synchronous machine action in the operational principles of all these doubly-fed machines.

ACKNOWLEDGMENT

The authors would like to acknowledge supports from Jerry Lloyd, Gerry Baker, Keith Hoemann and John Kondracki of Emerson Motor Co., Helmuth Glatt and Bob Landgraf of US Electric Motors, Prof. D.W. Novotny and Chiping Sun of UW-Madison during prototyping and testing of the DFRM/Drive.

REFERENCES

[1] A. Kusko and C.B. Somuah,"Speed Control of a Single Frame Cascade Induction Motor with Slip-Power Pump Back", *IEEE Trans. on Industrial Applications,* vol.IA-14,no.2 1979, pp.97-105

[2] F. Shibata and T. Kohrin,"A Brushless, Self-Excited Polyphase Synchronous Generator", *IEEE Trans. on Power Apparatus and Systems,* vol.PAS-102,no.8, 1983

[3] C.J. Heyne and A.M. El-Antably, "Reluctance and Doubly-Excited Reluctance Motors", Final Report to Oak Ridge National Lab, ORNL/SUB/8195013/1

[4] F. Liang, L.Xu and T.A. Lipo,"D-Q Analysis of a Variable Speed Doubly AC Excited Reluctance Motor", *Electric Machines and Power Systems*, vol.19, no.2, March 1991,pp.125-138

[5] L. Xu, F. Liang and T.A. Lipo,"Transient Model of a Doubly Excited Reluctance Motor", *IEEE Trans. on Energy Conversion*, vol.6,no.1 March 1991, pp.126-133

[6] L.Xu,"Analysis of a Doubly-Excited Brushless Reluctance Machine by FEA", IEEE IAS Annual Meeting, Houston, Texas, 1992, pp. 171-177

[7] L.Xu and Y. Tang,"A Novel Wind-Power generating System using Field Orientation Controlled Doubly-Excited Brushless Reluctance Machine", ibid., pp. 408-413

[8] R. Li, R. Spee, A.K.Wallace and G.C. Alexander," Synchronous Drive Performance of Brushless Doubly-Fed Motors", ibid., pp. 631-638

[9] W. Brassfield, R. Spee and T. Habetler,"Direct Torque Control for Brushless Doubly-Fed Machines", ibid. p. 615-22

[10] C. Brune, R. Spee and A. Wallace," Experimental Evaluation of a Variable-Speed, Doubly-Fed Wind-Power Generation System", IEEE IAS Annual Meeting,1993, Toronto, pp. 480-87

[11] B.S. Perera and B.H. Smith,"Brushless Constant-Frequency Generation using Single-Frame Cascaded Induction Machines" *Electric Machines and Power Systems,* 19:399-413, 1991

[12] A.R.W. Broadway and L. Burbridge,"Self-Cascaded Machine: A Low speed Motor or High frequency Brushless Alternator", *PIEE*, vol. 117(7), 1970,pp.1277-1290

[13] A.R.W. Broadway,"Cageless Induction Motor", *PIEE*, vol. 118, 1971,pp.1593-1600

[14] Y. Liao," Sensorless Drive Control and Method of Doubly-Fed Reluctance Motor," U.S. Patent 08/014,254

[15] Y. Liao and C. Sun,"A Low Cost, Robust Position Sensorless Control Scheme for DFRM Drive", IEEE IAS Annual Meeting,1993, Toronto, pp. 437-44

[16] Y. Liao and J. Lloyd,"A Position Sensorless, Brushless Doubly-Fed Reluctance Motor Drive", to appear in IEEE IAS Annual Meeting, 1994, Denver, Colorado

[17] B. Heller and V. Hamata,"*Harmonic Field Effects in Induction Machines*", Elsevier Scientific Publishing Co., 1977

[18] N.L.Schmidt and D.W. Novotny : "*Introductory Electromechanics.*" Ronald Press, 1965

[19] L. Xu and Y. Liao,"Finite Element Analysis of the Effect of Cross-Coupling in Doubly-Fed Reluctance Machines", to appear in ICEM'94, Sept. 1994, Paris, France